IOP Publishing | Institute of Physics and Engineering in Medicine Physics in Medicine & Biology

Phys. Med. Biol. **60** (2015) 117–136 doi:10.1088/0031-9155/60/1/117

Simulation of triple coincidences in PET

J Cal-González[1,4], E Lage[2], E Herranz[1], E Vicente[1], J M Udias[1], S C Moore[3], M-A Park[3], S R Dave[2], V Parot[2] and J L Herraiz[2]

[1] Grupo de Física Nuclear, Dpto. de Física Atómica, Molecular y Nuclear, Universidad Complutense de Madrid, CEI Moncloa, Spain
[2] Madrid-MIT M+Visión Consortium, Research Lab. of Electronics, Massachusetts Institute of Technology, Cambridge, MA, USA
[3] Division of Nuclear Medicine, Department of Radiology, Harvard Medical School and Brigham and Women's Hospital, Boston, USA

E-mail: herraiz@mit.edu

Received 24 June 2014, revised 27 October 2014
Accepted for publication 29 October 2014
Published 5 December 2014

Abstract

Although current PET scanners are designed and optimized to detect double coincidence events, there is a significant amount of triple coincidences in any PET acquisition. Triple coincidences may arise from causes such as: inter-detector scatter (IDS), random triple interactions (R_T), or the detection of prompt gamma rays in coincidence with annihilation photons when non-pure positron-emitting radionuclides are used ($\beta^+\gamma$ events). Depending on the data acquisition settings of the PET scanner, these triple events are discarded or processed as a set of double coincidences if the energy of the three detected events is within the scanner's energy window. This latter option introduces noise in the data, as at most, only one of the possible lines-of-response defined by triple interactions corresponds to the line along which the decay occurred. Several novel works have pointed out the possibility of using triple events to increase the sensitivity of PET scanners or to expand PET imaging capabilities by allowing differentiation between radiotracers labeled with non-pure and pure positron-emitting radionuclides. In this work, we extended the Monte Carlo simulator PeneloPET to assess the proportion of triple coincidences in PET acquisitions and to evaluate their possible applications. We validated the results of the simulator against experimental data acquired with a modified version of a commercial preclinical PET/CT scanner, which was enabled to acquire and process triple-coincidence events. We used as figures of merit the energy spectra for double and triple coincidences and the triples-to-doubles ratio for different energy windows and radionuclides. After validation, the

[4] Author to whom any correspondence should be addressed. Present address: QIMP group, Center for Medical Physics and Biomedical Engineering, Medical University of Vienna, Austria.

simulator was used to predict the relative quantity of triple-coincidence events in two clinical scanners assuming different acquisition settings. Good agreement between simulations and preclinical experiments was found, with differences below 10% for most of the observables considered. For clinical scanners and pure positron emitters, we found that around 10% of the processed double events come from triple coincidences, increasing this ratio substantially for non-pure emitters (around 25% for ^{124}I and > 50% for ^{86}Y). For radiotracers labeled with ^{18}F we found that the relative quantity of IDS events in standard acquisitions is around 18% for the preclinical scanner and between 14 and 22% for the clinical scanners. For non-pure positron emitters like ^{124}I, we found a $\beta^+\gamma$ triples-to-doubles ratio of 2.5% in the preclinical scanner and of up to 4% in the clinical scanners.

Keywords: positron emission tomography, Monte Carlo Simulations, triple coincidences

(Some figures may appear in colour only in the online journal)

1. Introduction

Positron emission tomography (PET) scanners are designed to detect and record double coincidences originated by positron–electron annihilation photons. However, in any PET acquisition there is a significant amount of events in which three or more single photons are detected within the time coincidence and/or energy window of the scanner (Levin 2008). When non-pure positron emitters such as ^{124}I, ^{86}Y or ^{76}Br are used, the prompt gamma rays emitted simultaneously with positrons can be detected in coincidence with the annihilation gamma rays (Surti *et al* 2009, Belov *et al* 2011) giving rise to triple coincidences that we denominated positron-gamma ($\beta^+\gamma$) events (figure 1(*a*)). For both pure and non-pure positron-emitting radionuclides, it is also possible to detect random triple coincidences among photons originated by two (R_{T1}) (figure 1(*b*)), or three different annihilations (R_{T2}) (figure 1(c)). Moreover, triple coincidences are also caused by inter-detector scattered (IDS) events (figure 1(d)) in which one of the annihilation photons deposits energy in one detector and the other among at least two detectors. Finally, when the positron annihilates via formation of positronium in the triplet state ($^3S_1$, ortho-positronium), the disintegration of the ortho-positronium may result into the emission of three gamma-rays which can also create triple-coincidences (Harpen 2004, Kacperski and Spyrou 2005). In any of these cases, if the three photons are within the time and energy windows of the scanner, they may be discarded by the coincidence processor or alternatively, be processed as a set of double coincidences. In this later case, it will add noise to the data since at most only one of the three possible lines-of-responses (LORs) defined by the triple coincidence would correspond to the line along which a decay occurred. We want to note that coincidences of more than three events, as well as coincidences from ortho-positronium desintegrations, are very unlikely and have not been considered in this work.

During the last years, several works have evaluated the possibility of using triple coincidences to enhance the performance of PET scanners and increase their capabilities. For example, the detection of triple coincidences may be used to differentiate a radiotracer labeled with a pure positron emitter from another labeled with a positron-gamma emitter, thus enabling dual-tracer PET (Andreyev and Celler 2011, Sitek *et al* 2011, Andreyev *et al* 2012, Parot *et al*

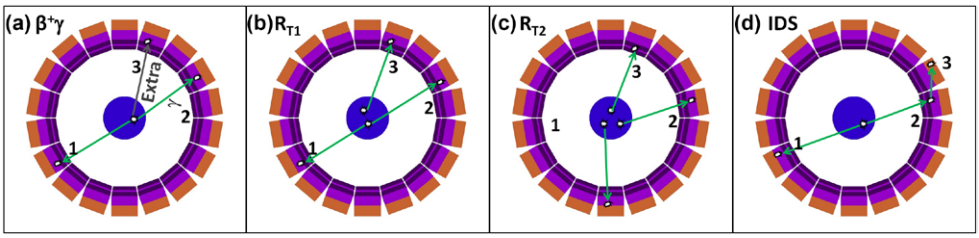

Figure 1. Different types of triple coincidences that may occur in PET acquisitions. (*a*) $\beta^+\gamma$: detection in coincidence of an extra (prompt) gamma ray and two annihilation photons. (*b*) R_{T1}: random triple event from two disintegrations. (*c*) R_{T2}: random triple event from three different decays. (*d*) IDS: inter-detector scatter event: one of the annihilation photons deposits energy in one detector and the other among at least two detectors. IDS, R_{T1} and R_{T2} events may occur both for pure and non-pure β^+ emitters while $\beta^+\gamma$ events only take place for non-pure β^+ emitters.

2013). On the other hand, IDS (Rafecas *et al* 2003, Levin 2008, Clerk-Lamalice *et al* 2012, Gillam *et al* 2012, Wagadarikar *et al* 2012, Lage *et al* 2014, Gillam *et al* 2014) or even R_{T1} and $\beta^+\gamma$ triple events (Lin *et al* 2012, Robinson *et al* 2004, Lage *et al* 2014) can be used for increasing the photon sensitivity of PET scanners, thus enabling reduction in acquisition times and/or dose to the patient.

In order to evaluate the relevance of triple coincidences in PET acquisitions and to determine the scanner settings that would be optimal to register or filter these events, it is useful to have a complete and accurate model of the emission and detection of the radiation. Monte Carlo (MC) simulations are commonly used for this task (Buvat and Lazaro 2006) because they allow tracking all possible emissions and interactions. Nevertheless, as triple coincidences are not usually considered in PET acquisitions, these MC simulators require some modifications and additional tools to analyze the simulation results. PeneloPET (España *et al* 2009) is a MC simulation software based on Penelope (Baró *et al* 1995, Salvat *et al* 2008) which is fast, flexible and easy to use. Although Penelope is less generally aimed than other simulation packages such as GEANT4 (Agostinelli 2003, Allison *et al* 2006) or GATE (Jan *et al* 2004, 2011), it suits PET needs well and has been used for several medical physics applications (Sempau and Andreo 2006, Panettieri *et al* 2007, Abushab *et al* 2011).

The goal of this work was to extend PeneloPET to include tracking and analysis of triple coincidences in PET scanners. To validate the simulator, we compared our results against experimental measurements performed in a preclinical PET/CT scanner modified to be capable of acquiring, storing and analyzing multiple coincidences. Once validated, we used our simulator to predict the quantity and evaluate the effect of triple coincidences in several situations (different energy windows and radionuclides) for the preclinical scanner and for two clinical scanners: the Siemens Biograph True Point PET/CT with TrueV (TPTV) and the GE Discovery-690.

2. Methods

2.1. MC simulations with PeneloPET

2.1.1. PeneloPET code. PeneloPET is an easy-to-use simulation software which allows accurate simulation of different PET systems. This can be done by modifying some configuration files containing parameters related to detector geometries and acquisition settings such as coincidence and energy windows. Moreover, this software is capable of accurately simulate

different imaging situations by allowing the definition of voxelized or geometrical sources. During simulations, PeneloPET takes into account the main physical effects of interest in PET such as positron range, non-colinearity of the gamma photons and attenuation and scatter in the body and in the scanner. It can generate list-mode files with detailed information which can be analyzed and reconstructed as in an actual PET scanner. Furthermore, in the new release of this software (v3.0, released in 2014 and freely available under request[5]) each photon is associated with a specific decay, enabling the detection and classification of double, triple and higher-order interactions.

2.1.2. Prompt-gamma emitting radionuclides. The decay scheme of several PET radionuclides of interest (^{68}Ga, ^{82}Rb, ^{124}I, ^{76}Br, ^{86}Y, ^{94}Tc, ^{94m}Tc, ^{60}Cu and ^{61}Cu) was included in this new release of PeneloPET using data obtained from nuclear databases (NNDC 2011). Only cascades with a branching ratio (number of times that a certain decay mode occurs per disintegration) greater than 2% and gamma photon emissions with a branching ratio greater than 1% were considered. The half-life of the intermediate excited states in the daughter nuclei, being always less than 100 ps, was neglected in all the cases since this short half-life is usually much lower than the typical timing resolution of current PET scanners.

For some of the radionuclides considered in this work, there is a large fraction of the decays that occur without the emission of a positron in a process known as Electron Capture (EC) decay (Krane 1987). The new simulation code samples the decay scheme of the radionuclide and generates tracks for each cascade with the corresponding probability. In this way, positrons and γ photons emitted in each decay cascade are taken into account in the simulation.

Table 1 shows the percentage of gamma-rays emitted by the non-pure β^+ emitters considered in this work, including the percent of times that the radionuclide decays in a certain way (β^+ emission or EC) and the energy and quantity of the most probable prompt gamma ray emitted in coincidence with positrons. To provide an intuitive idea about the effect that the extra emissions from these radionuclides might have in a PET acquisition, we also included information about these prompt gamma rays, in coincidence or not with the positron emission, with an energy below, within or above the typical energy window used in PET systems (400–650 keV).

2.2. Simulation models

2.2.1. Preclinical scanner. To validate our simulation software we used the Argus small-animal PET/CT scanner (Sedecal S.A. Madrid, Spain) which was formerly distributed by General Electric under the name eXplore Vista/CT (Wang *et al* 2006). This system consists of 36 block detectors, each one comprised of a square position sensitive photomultiplier tube (PS-PMT) coupled to a dual layer array of 13 × 13 LYSO + GSO scintillation crystals. Each crystal in the array has a cross section of 1.45 × 1.45 mm^2 and is wrapped in all the faces except one with a 0.1 mm thickness white reflector. The resulting pitch size of each crystal in the array is 1.55 mm and the length of the LYSO and GSO layers is 7 mm and 8 mm, respectively. The 36 modules are arranged in two rings of 18 modules each, with a diameter of 11.8 cm. Each detector-module is in coincidence with 14 opposing modules (seven in its own ring and seven in the other ring). This configuration provides a transaxial field of view (FOV) of 67 mm and axial FOV of 48 mm.

The acquisition software of the Argus scanner was adapted to provide list-mode data files with all the detected single events within a coarse coincidence window (±10 ns) and an

[5] See http://nuclear.fis.ucm.es/penelopet for details.

Table 1. Energy distribution of the γ emissions for the $\beta^+\gamma$ emitting radionuclides considered in this work.

Radionuclide	Ratio β^+ (%)	Ratio EC (%)	Main γ energy (yield %)	γ emissions: in coincidence with β^+ / Not in coincidence (% per decay)			
				< 400 keV	400–650 keV	> 650 keV	Total
^{22}Na	90.4	9.6	1275 (100%)	0.0 / 0.0	0.0 / 0.0	90.4 / 9.5	90.4 / 9.5
^{68}Ga	88.9	11.1	1080 (3%)	0.0 / 0.0	0.0 / 0.0	1.2 / 2.2	1.2 / 2.2
^{82}Rb	95.4	4.6	777 (13%)	0.0 / 0.0	0.0 / 0.0	13.1 / 2.6	13.1 / 2.6
^{94m}Tc	70.2	29.8	871 (94%)	0.0 / 0.0	0.0 / 0.0	70.2 / 37.1	70.2 / 37.1
^{124}I	22.7	77.3	602 (61%)	0.0 / 0.0	11.9 / 43.0	0.5 / 27.7	12.4 / 70.7
^{76}Br	55.0	45.0	559 (74%)	0.0 / 0.0	71.8 / 2.4	34.8 / 25.6	106.6[a] / 28.0
^{86}Y	31.9	68.1	1080 (83%)	3.2 / 5.0	37.9 / 33.9	133.3*/61.0	174.4[a] / 99.9

[a] A percentage greater than 100% means that more than one gamma ray are emitted per decay.

80-to-1400 keV energy window. Each single event in the file contains energy and position information and coarse plus fine time-stamps, which allows the identification of coincidences from two, three or more events. This file can be processed to create several different datasets, for example, one containing only double coincidences and another with triple coincidences. To be classified as valid coincidences, and consequently recorded, coincidence events have to be within user-specified energy and timing windows. The timing window used in the experimental and simulation measurements was: 5 ns for LYSO–LYSO, 7 ns for LYSO -GSO and 10 ns for GSO–GSO layers.

The average energy and timing resolution for 511 keV photons used in the simulation model of the scanner were those previously reported by Wang *et al* (Wang *et al* 2006). In addition, we included in our simulator a non-uniformity factor for each detector, to take into account differences in energy resolution and gain between different scintillator crystals. These non-uniformity factors were computed by fitting the simulated spectra to the measured ones for all the singles acquired in a calibration acquisition. A ^{68}Ge ring phantom uniformly covering the FOV of the scanner, which is the source used in this scanner to calculate standard normalization corrections, was used to obtain the calibration data. Two free parameters were set to be adjusted: one to model differences in gain between crystals and another taking into account differences in the sensitivity of each scintillator crystal. These fitting parameters were later used to obtain the spectra for double and triple coincidences and for all the radionuclides studied in this work.

2.2.2. Clinical scanners. Two clinical scanners have been considered in this study: the Siemens Biograph TruePoint TrueV (B-TPTV) and the GE Discovery-690. To create the simulation model of the Biograph TPTV scanner, we used previously published values for geometries, energy, and timing windows (Jakoby *et al* 2009). The scanner consists of four 48-detector rings providing an axial FOV of 21.8 cm and a transaxial FOV of 68.4 cm (each detector is in coincidence with another 25 detectors). Each block-detector comprises a 13 × 13 matrix of 4 × 4 × 20 mm^3 lutetium oxyorthosilicate scintillator crystals coupled to four photomultiplier tubes. The scanner operates only in three-dimensional (3D) mode with an axial coincidence acceptance of ±38 planes. Data are acquired with a 4.5 ns coincidence time window and an energy window of 425–650 keV.

The other clinical scanner considered in this work, the GE Discovery-690 (Bettinardi *et al* 2011), consists of four rings of detectors providing an axial FOV of 15.7 cm and a transaxial FOV of 70 cm (all detectors are in coincidence with each other). The PET detection unit

consists of a 9 × 6 matrix of individual LYSO crystals (each crystal is 4.2 × 6.3 × 25 mm^3) coupled to a single squared PS-PMT with four anodes. As the Biograph TPTV scanner, the Discovery-690 operates only in 3D mode with an axial coincidence acceptance of ±23 planes. The energy window is 425–650 keV and the coincidence time window is 4.9 ns.

In the simulation of these scanners we did not take into account the differences in energy resolution and gain between different scintillator crystals. We used instead published values of energy and timing resolution as a global contribution for all detectors (11.5% and 528 ps for the Biograph TPTV and 12.4% and 544 ps for the GE Discovery-690).

2.2.3. Modeling the electronics of the PET systems. Besides geometry and materials, PeneloPET includes in the simulations several factors related to acquisition electronics which allows an accurate modeling of the scanner performance. Those factors include single and coincidences dead time, integration time and pile-up effects among others. However, in order to mimic the behavior of the PET scanners simulated in this work, where in most cases the full details of the electronics were not known, we adjusted the singles dead time to reproduce the experimental random, prompt and noise equivalent count rate (NECr) curves of these systems.

2.3. Validation of the new release of PeneloPET

We first validated the new version of PeneloPET and the simulation model of the scanners for double coincidences by comparing the sensitivity, scatter fraction (SF) and noise equivalent count rate (NECr) curves obtained from the simulator with the experimental values obtained from the Argus scanner and with the values reported in the literature for the clinical scanners.

To validate the performance of PeneloPET for triple coincidences we compared the output of the simulation with phantom measurements obtained using pure and non-pure positron$^-$ emitting radionuclides in the Argus scanner. As figures of merit in the validation we have used the ratio of triple-to-double coincidences for different scanner settings and the energy spectra for double and triple coincidences.

2.3.1. Analysis of experimental and simulated data. To analyze the output data from the Argus scanner we developed an analysis software tool which reads the singles list-mode data and classify the events into double, triple and multiple (more than three singles) coincidences. A similar program was developed to sort the singles list-mode data obtained from the simulations. With these software tools, the user can choose different parameters (such as timing or energy windows) to define different selection criteria for double and triple coincidences. In our specific case, energy windows for measured and simulated data were set as follows:

- Double coincidences (EW_D): we used a 400–700 keV energy window for the Argus scanner and a 425–650 keV for the Biograph and Discovery scanners. In the experimental data, we obtained the proportion of prompt and random coincidences within this energy window (EW_D). In the simulation, double coincidences were tagged as True (T), Scatter (Sc), Random (R_D) or Double $\beta^+\gamma$ (spureous coincidence of an annihilation gamma ray with a prompt gamma) events (Beattie *et al* 2003, Lubberink and Herzog 2011).

For triple coincidences we used three different criteria optimized to identify IDS, $\beta^+\gamma$ and R_T events, respectively:

- IDS events ($EW_{T\text{-}IDS}$): the energy of one single and the sum of the other two should be within the EW_D.

- $B^+\gamma$ events ($EW_{T\text{-}\beta\gamma}$): two singles should be within the EW_D and the third single should be above a threshold selected according to the energy of the prompt gamma ray. This threshold was set to the upper limit of the EW_D when the extra gamma rays had much higher energy than 511 keV (^{22}Na, ^{82}Rb or ^{94m}Tc radionuclides) or to the lower limit of the EW_D if the extra gamma rays have an energy which is close to 511 keV (^{124}I, ^{76}Br or ^{86}Y radionuclides).
- R_T events ($EW_{T\text{-}RT}$): The three singles should be within the EW_D.

Note that more than one type of triple coincidences might be within a given energy window. For example, for a non-pure emitter such as ^{124}I, which has a main extra gamma ray of 603 keV (table 1), there will be R_T events, as well as $\beta^+\gamma$ events, in the $EW_{T\text{-}\beta\gamma}$ window that we cannot differentiate in the experimental data but can be differentiated in the simulations. Regarding IDS events, since all the scanners simulated in this work are based on block detectors and with this configuration it is not possible to differentiate simultaneous multiple interactions within the same block, it is a requisite that in each triple coincidence every single photon has to be detected in a different block. Note however that, although not included in this work, the simulator is perfectly capable of detecting multiple interactions in the same block.

2.3.2. Argus PET/CT preclinical scanner: experimental measurements and simulations. We performed measurements and simulations in the Argus scanner to determine sensitivity, SF and NECr. In all these tests we used only double coincidences (all other multiple coincidences were discarded) and followed the guidelines described in the NEMA NU-4 protocol (NEMA NU-4 2008) which is designed to measure the performance of preclinical PET scanners in a standard way.

Sensitivity was evaluated by measuring and simulating an encapsulated 0.13 MBq ^{22}Na point source carefully centered in the FOV. Since ^{22}Na is a $\beta^+\gamma$ emitter, this acquisition was also used to compare the fraction of triple coincidences in real data and simulations. The SF and NEC rates of the scanner were obtained for mouse-sized objects. We measured and simulated acquisitions of a 7 cm long and 2.5 cm diameter polyethylene cylinder positioned in the isocenter of the FOV. A line source was filled with ^{18}F and inserted axially into a hole of the phantom located 1 cm below its central axis. The initial activity of the line source was 2 MBq ml^{-1} and the total acquisition time was 7 times the half-life of this radionuclide. The SF was obtained at the end of the acquisition, with very low activity in the phantom.

To validate the simulator for triple coincidences we compared the fraction of triple coincidences in typical PET acquisitions by measuring and simulating a NEMA image quality (IQ) phantom (NEMA NU-4 2008) filled with one of ^{18}F (3.4 MBq), ^{124}I (7.84 MBq) or ^{76}Br (3.89 MBq).

The figures of merit evaluated to validate our simulation of triple coincidences were

- Averaged energy spectra for singles, doubles and triple coincidences in all LYSO and GSO scintillator crystals.
- Statistics of triple coincidences within each of the considered energy windows for triples.

After validation, we evaluated by means of MC simulations, the statistics of triple events within different energy windows for standard acquisitions using the following radionuclides: ^{68}Ga, ^{82}Rb, ^{94m}Tc and ^{86}Y. The phantom simulated in these experiments was, as in the previous case, a NEMA IQ phantom filled with a total activity of 3.5 MBq. Finally, we estimated the variation of the triple coincidence rate with the activity concentration for representative pure (^{18}F) and non-pure (^{124}I) positron-emitting radionuclides.

2.3.3. PeneloPET simulations of clinical scanners. To validate the simulation models of the Biograph TPTV and the Discovery-690 PET scanners we simulated the sensitivity, SF and NECr curves of these systems following the NEMA protocol for clinical scanners (NEMA NU-2 2007). Afterwards, we compared the results of our simulation with the experimental values reported by (Jakoby *et al* 2009) for the Biograph and from (Bettinardi *et al* 2011) for the Discovery. The sensitivity was measured by simulating a line source (70 cm length) placed at the center of the FOV. SF and NECr curves were obtained from the simulations of a 70 cm long and 20 cm diameter polyethylene cylinder, positioned in the isocenter of the FOV. The phantom contained a line source filled with ^{18}F (with an initial activity concentration of 45 kBq ml^{-1}) inserted axially into a cylindrical hole located 4.5 cm below the central axis of the phantom.

After the validation of the simulation models of these scanners, we used PeneloPET to estimate the proportion of triple coincidences for several radionuclides (^{18}F, ^{124}I and ^{86}Y). Again, we evaluated energy spectra for double and triple coincidences and the relative proportion of triple coincidences in different energy windows. The energy spectra were obtained from the simulation of a 200 kBq point source placed in the center of the FOV. The relative abundance of each type of triple coincidences was estimated using the previously described NEC phantom with a 0.5 kBq ml^{-1} activity concentration, which is concordant with the doses used in standard clinical acquisitions (^{18}F-FDG). We also studied, using the same phantom, the behavior of the triple-to-double coincidences ratio as a function of the activity concentration for representative pure (^{18}F) and non-pure (^{124}I) PET radionuclides.

Finally, we estimated the number of triples which fall within the EW_D and would be processed as double coincidences if the scanner does not discard multiple coincidence events. To do so, we simulated several acquisitions of the same phantom used in the NECr measurements filled with ^{18}F, ^{124}I or ^{86}Y at activity concentrations ranging from 0.05 to 35 kBq ml^{-1}. List-mode data produced by the simulator were processed to determine the number of cases in which two or three photons coming from a specific type of triple interaction fall within the EW_D and consequently, may be included as two or three LORs in the doubles dataset.

2.3.4. Uncertainties in simulated and experimental data. Systematic uncertainty in the case of the real measurements, and the simulations tuned to reproduce them, is dominated by the uncertainty in the true value of the activity and the exact location of the sources employed in the measurements. Since this value was on the order of 5% for all the experiments presented in this work, this translates into a 5% systematic uncertainty in sensitivities, peak NEC rates, and also in the total number of coincidences of each type. Moreover, statistical errors have been computed as the square root of the number of events of each type in each energy window. The final uncertainty value shown in all the tables of this paper has been calculated as the quadratic sum of the statistical error and the 5% systematic error.

3. Results

3.1. Validation of PeneloPET in double coincidences mode

As mentioned before, the effective dead time used in the simulation model of each clinical scanner was first computed by fitting the simulated NECr curves of each system to the experimental values reported in the literature. We obtained good fits to the experimental data using a 50 ns effective dead time for the Biograph and 100 ns for the Discovery. For the Argus scanner we used a previously reported simulation model (España *et al* 2009) with a 2 ms effective dead time.

Figure 2 shows the simulated and experimental NEC curves for the Argus scanner (mouse phantom) and for the Biograph and GE clinical scanners (NEMA protocol), whereas tables 2

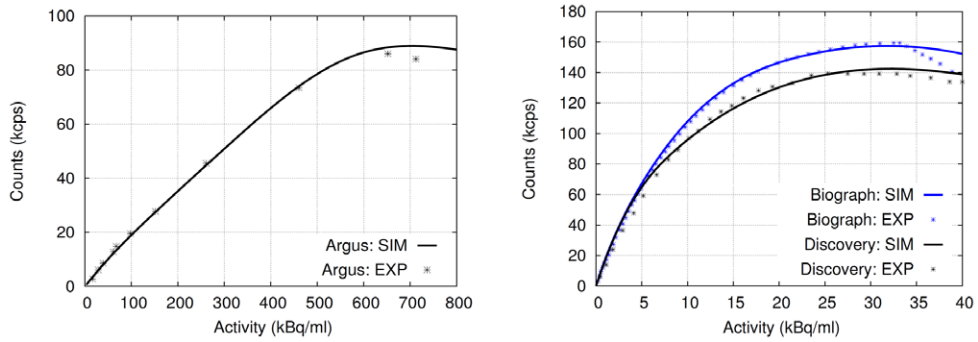

Figure 2. Simulated and measured NEC curves for the preclinical Argus scanner (left) and for the clinical Biograph TPTV and GE Discovery-690 scanners (right).

Table 2. NEC peak rates and SF for the scanners considered in this work.

	NEC (Kcps) @(kBq ml^{-1})		Scatter fraction (%)	
Scanner	Simulated	Experimental	Simulated	Experimental
Biograph TPTV	157 ± 8 @ 32 ± 2	161 ± 8 @ 31 ± 2[a]	33.0 ± 1.7	32.5 ± 1.7[a]
GE discovery-690	142 ± 7 @ 32 ± 2	139 ± 7 @ 29 ± 2[b]	35.0 ± 1.8	37.0 ± 1.9[b]
Argus (mouse phantom)	89 ± 5 @ (700 ± 40)	88 ± 4 @ (690 ± 30)	13.5 ± 0.7	13.9 ± 0.7

[a] Jakoby *et al* 2009.
[b] Bettinardi *et al* 2011.

Table 3. Sensitivity for the scanners considered in this work.

	Energy window (keV)	Sensitivity (%) @ at the center	
Scanner		Simulated	Experimental
Biograph TPTV	425–650	0.82 ± 0.04	0.81 ± 0.04[a]
GE Discovery-690	425–650	0.74 ± 0.04	0.74 ± 0.04[b]
Argus	400–700	2.09 ± 0.11	2.06 ± 0.11

[a] Jakoby *et al* 2009.
[b] Bettinardi *et al* 2011.

and 3 compare simulated and experimental data for peak NEC rates, SF and sensitivity in the three scanners. As shown in figure 2, count rate performance of these scanners is well reproduced by the simulator for activities under the NEC peak rates (discrepancies below 10% in all the cases). For activities beyond the NEC peak, the simulations tend to overestimate the experimental curve, likely due to additional bottlenecks in the data processing not considered in the simulations. The results presented in tables 2 and 3 also show a good agreement between simulations and measured values, with discrepancies smaller than 5% in sensitivity and SF, and than 10% in the peak NEC rate estimations.

3.2. Validation of the simulation tool for Triple coincidences

3.2.1. Energy spectra for double and triple coincidences in the Argus scanner. Figure 3 compares simulated and measured energy spectra of several radionuclides (^{18}F, ^{22}Na, ^{124}I and ^{76}Br)

in the Argus scanner. Note that we present separated energy spectra for the LYSO and GSO layers of the detectors (left column), and for double and triple coincidences (right column). Spectra of double and triple coincidences have been scaled to a value of 1 in the photopeak (511 keV) for double coincidences. In addition, table 4 shows measured and simulated energy resolution (FWHM in %) at 511 keV for each radionuclide (averaged spectra for all crystals). Discrepancies in energy resolution for all the radionuclides evaluated are below 7%.

As we can see in figure 3, there is a good fit between simulated and measured energy spectra for all the radionuclides except for ^{76}Br, which shows noticeable discrepancies at energies below 400 keV. In this latter case, we confirmed with the ^{76}Br provider (Isotope Production Group at Washington University, St. Louis) that these discrepancies were caused by the presence of non-negligible levels of radioactive contaminants (other Br radionuclides generated during the production procedure) in the experimental source which were not considered in the simulation.

3.2.2. Counting statistics of triple coincidences in the Argus scanner. In table 5 we summarized the counting statistics for double and triple coincidences in the Argus scanner (experimental and simulated values). The first row of the table contains the results for double coincidences in thousands of counts per second (kcps) per MBq of activity. For the experimental results we indicated the percentage of Prompt and Random events which were found in the data, while for simulated data, we also included the relative percentages of true, scattered, doubles $\beta + \gamma$ and double random events in the doubles dataset. Rows 2–5 contains statistics for triple events within each energy window considered for triple coincidences. The first two lines of rows 2–5 indicates the experimental and simulated rate of triple coincidences (kcps MBq^{-1}) in each specific energy window, while the remaining lines indicate the contribution (%) of each type of triple coincidence (IDS, $\beta^+\gamma$, R_{T1}, $R_{T2,}$ see also figure 1) to the rate of triples obtained from the simulator.

For double-coincidence events, we found an excellent agreement between simulation and experiments for all the radionuclides evaluated (discrepancies between experimental and simulated count rates smaller than 2%). Triple-to-double ratios for the IDS ($EW_{T\text{-}IDS}$) and random-triple ($EW_{T\text{-}RT}$) energy windows were also in good agreement (~10% discrepancies in the worst case) with simulations for all the radionuclides except for ^{76}Br. In this latter case, as it was described in section 3.2.1, the differences between measurements and simulations can be explained by the presence of radioactive contaminants in the ^{76}Br source. In the energy window optimized for $\beta^+\gamma$ triple coincidences ($EW_{T\text{-}\beta\gamma}$) we also found a good agreement (~10% discrepancies in the worst case) between simulated and experimental data, even for ^{76}Br. Note that except for ^{22}Na, which has a 1275 keV extra gamma ray, the prompt gamma rays emitted by ^{124}I (602 keV) and ^{76}Br (559 keV), cannot be differentiated in terms of energy from annihilation photons.

3.2.3. Relative abundance of triple coincidences as a function of the activity within the FOV. We used the simulator to study the relative proportion of each type of triple coincidence in the Argus scanner as a function of the total activity within the FOV. Figure 4 shows the results of this simulation for reference pure and non-pure positron emitters (^{18}F and ^{124}I, respectively). As expected, for both types of radionuclides, the R_T event rate increases with the activity within the FOV, while the IDS event rate, which depends on the geometry and characteristics of the scanner, is not affected by this parameter.

It is noticeable that there is always a certain rate of R_T events falling within the $EW_{T\text{-}\beta\gamma}$ and $EW_{T\text{-}IDS}$ energy windows that increases with activity concentration. Since the most probable prompt gamma emitted by ^{124}I has 602 keV, the Argus scanner cannot distinguish $\beta^+\gamma$ triple

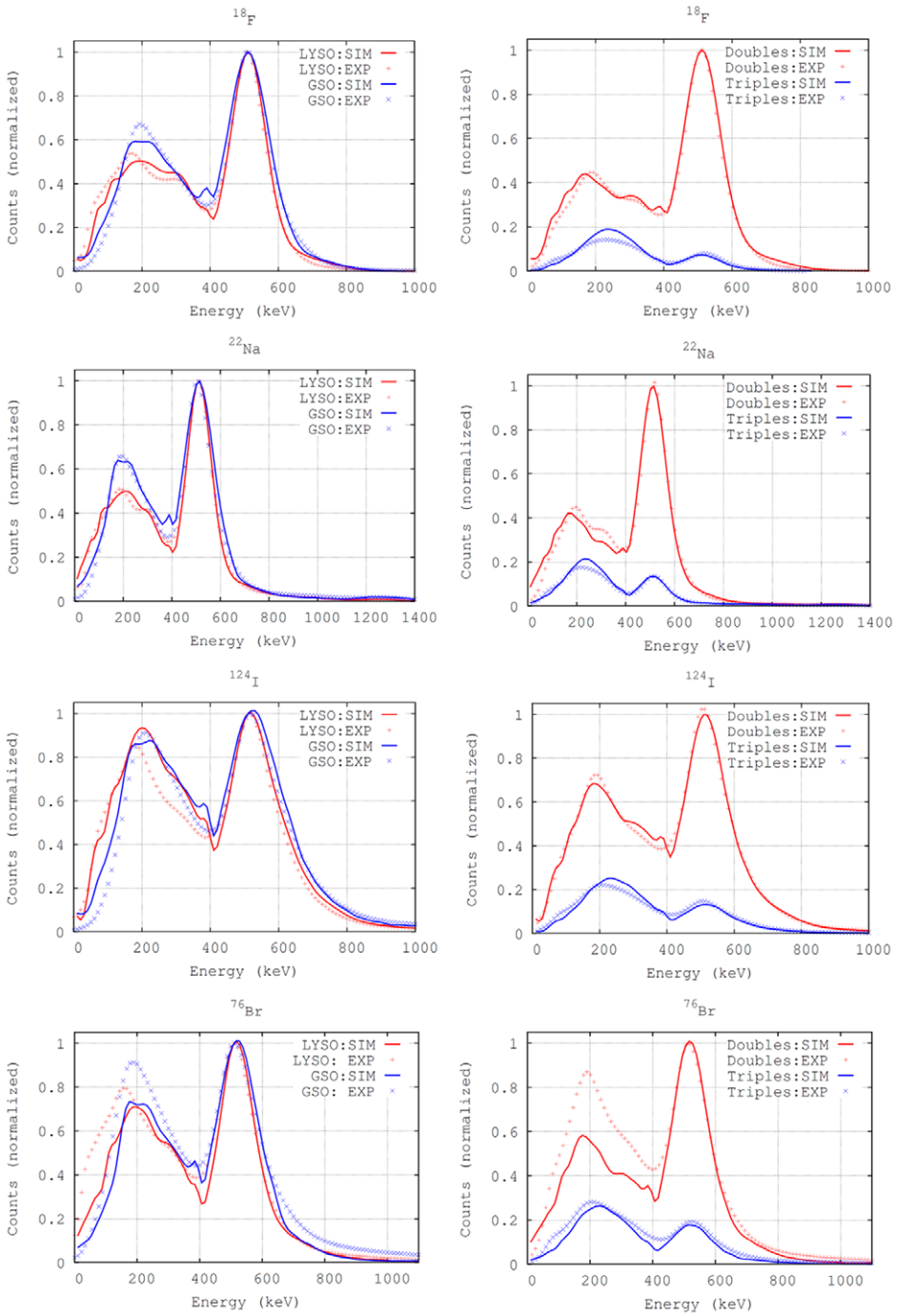

Figure 3. Simulated (solid lines) and measured (dotted lines) energy spectra for the Argus scanner. Radionuclides from top to bottom are ^{18}F, ^{22}Na, ^{124}I and ^{76}Br. On the left side, the energy spectra for all singles interacting in the LYSO (red) and GSO (blue) layers are shown. On the right side, we depict the energy spectra for double (red) and triple (blue) coincidences.

Table 4. Full width at half maximum (FWHM) of the full energy peaks at 511 keV for LYSO and GSO scintillator crystals in the Argus scanner.

	FWHM @ 511 keV (%) (Measured / Simulated)			
	^{18}F	^{22}Na	^{124}I	^{76}Br
LYSO	(25.5 / 25.3) ± 1.3	(26.2 / 25.8) ± 1.3	(34.0 / 35.0) ± 1.8	(30.6 / 29.2) ± 1.5
GSO	(28.2 / 29.9) ± 1.5	(28.3 / 30.1) ± 1.5	(37.2 / 38.1) ± 1.9	(34.9 / 33.9) ± 1.8

events from R_T events for this radionuclide. Furthermore, R_T events detected within $EW_{T\text{-}IDS}$ may come from different sources such as R_T or $\beta^+\gamma$ events in which two of the photons scatter in the object before being detected.

It is also interesting to note that for the pure positron emitter, the R_{T1} and IDS events can be effectively detected using the energy-based criteria described in section 2.3.1 without a significative contamination from R_T events in $EW_{T\text{-}IDS}$ and from R_{T2} in $EW_{T\text{-}RT}$ (figure 3, top plots). This simulation also points out that for a mouse-sized object (used in this case), the R_T event rate in pure and non-pure emitters is mainly due to R_{T1} events and that R_{T2} events are only significative at high activity concentrations.

To summarize, figure 5 shows a comparison between the total triples-to-doubles ratio for ^{18}F and ^{124}I in the same energy windows.

3.2.4. Evaluation of triple coincidences for other radionuclides. The rate of triple coincidences in the Argus scanner for other non-pure radionuclides of interest (^{68}Ga, ^{82}Rb, ^{94m}Tc and ^{86}Y) was also evaluated using the simulator (table 6).

Although ^{68}Ga is, strictly speaking, a positron-gamma emitter, the probability of emission of the extra gamma ray (1080 keV) in coincidence with the positron is so small (3%) that it behaves very similarly to the pure positron emitter ^{18}F. ^{82}Rb and ^{94m}Tc have a relative high yield of positron emissions and a main extra gamma ray that can be differentiated from annihilation photons better than those emitted by ^{124}I or ^{76}Br (see table 1). The effect of this property can be seen in the lower percentage of double $\beta^+\gamma$ coincidences obtained for these radionuclides (table 6, row 1). The much higher percentage of double and triple $\beta^+\gamma$ events obtained for ^{86}Y is due to the high yield of extra emissions in this radionuclide, which on average emits more than one prompt gamma ray per decay.

Regarding the statistics for triple coincidences shown in tables 5 and 6, we can see that, except for ^{82}Rb, most triples detected in the $EW_{T\text{-}RT}$ and in the $EW_{T\text{-}\beta\gamma}$ are due to $\beta^+\gamma$ events with a very small contribution from R_T events. ^{82}Rb behaves differently because the relative yield of prompt gamma emissions (13%) for this radionuclide is significantly smaller than for the other non-pure emitters.

3.3. Simulation of triple coincidences in clinical scanners

3.3.1. Energy spectra for clinical scanners. In figure 6 we plotted the simulated energy spectra for double and triple coincidences in the Biograph and Discovery scanners. Since block detectors in clinical scanners use larger crystals, they have better efficiency for detection of 511 keV and higher energy photons and a better energy resolution than the preclinical scanner. These results indicate that clinical systems are better suited than the preclinical scanner to deal with triple coincidences, since their energy resolution provides a means for a better detection and classification of these types of events.

Table 5. Counting statistics for double and triple coincidences for ^{18}F, ^{22}Na, ^{124}I, and ^{76}Br (Argus scanner).

Energy window	Type of coincidence	^{18}F (3.40 MBq)	^{22}Na (0.13 MBq)	^{124}I (7.84 MBq)	^{76}Br (3.89 MBq)
EW_D	Doubles Exp (kcps MBq^{-1})	9.2 ± 0.5	17.7 ± 1.3	2.56 ± 0.14	4.2 ± 0.2
	Prompts (%)	99.4	99.5	98.8	98.7
	Randoms (%)	0.6	0.5	1.2	1.3
	Doubles Sim (kcps MBq^{-1})	9.3 ± 0.5	18.5 ± 1.3	2.55 ± 0.14	4.1 ± 0.2
	Trues (%)	87.5	87.7	67.5	64.9
	Sc (%)	11.5	6.4	10.0	10.7
	Doubles $\beta^+\gamma$ (%)	0.0	5.8	20.0	23.2
	R_D (%)	1.0	0.1	2.5	1.2
$EW_{T\text{-}IDS}$	Triples Exp (kcps MBq^{-1})	1.59 ± 0.09	3.4 ± 0.3	0.61 ± 0.04	1.26 ± 0.08
	Triples Sim (kcps MBq^{-1})	1.76 ± 0.12	3.8 ± 0.4	0.59 ± 0.04	1.00 ± 0.08
	IDS (%)	96.8	89.1	67.6	66.1
	$\beta^+\gamma$ (%)	0.3	10.9	26.9	32.1
	R_{T1} (%)	2.0	<0.1	2.9	1.1
	R_{T2} (%)	0.9	<0.1	2.6	0.7
$EW_{T\text{-}RT}$	Triples Exp (kcps MBq^{-1})	0.038 ± 0.006	0.25 ± 0.05	0.059 ± 0.005	0.129 ± 0.013
	Triples Sim (kcps MBq^{-1})	0.029 ± 0.006	0.30 ± 0.06	0.061 ± 0.006	0.165 ± 0.015
	$\beta^+\gamma$ (%)	<0.1	99.5	82.6	95.4
	R_{T1} (%)	99.2	0.5	15.8	4.0
	R_{T2} (%)	0.8	<0.1	1.6	0.6
$EW_{T\text{-}\beta\gamma}$ (^{22}Na)	Triples Exp (kcps MBq^{-1})	—	0.44 ± 0.11	—	—
	Triples Sim (kcps MBq^{-1})	—	0.51 ± 0.12	—	—
	$\beta^+\gamma$ (%)	—	99.9	—	—
	R_{T1} (%)	—	0.1	—	—
	R_{T2} (%)	—	<0.1	—	—
$EW_{T\text{-}\beta\gamma}$ (^{124}I, ^{76}Br)	Triples Exp (kcps MBq^{-1})	—	—	0.078 ± 0.008	0.198 ± 0.018
	Triples Sim (kcps MBq^{-1})	—	—	0.079 ± 0.009	0.195 ± 0.018
	$\beta^+\gamma$ (%)	—	—	82.3	95.0
	R_{T1} (%)	—	—	16.3	4.4
	R_{T2} (%)	—	—	1.4	0.6

3.3.2. Counting Statistics for double and triple coincidences in the clinical scanners. To the best of our knowledge, most clinical PET scanners do not process triple coincidences in a separate and specific way; they simply process the data to find photon pairs within predetermined time and energy windows. This means that for IDS events the scanner will record a double coincidence only if one of the two IDS photons (2 or 3 in (figure 1(d))) deposits energy above the low energy threshold of the scanner. Note that in this case, the correct lines-of-response

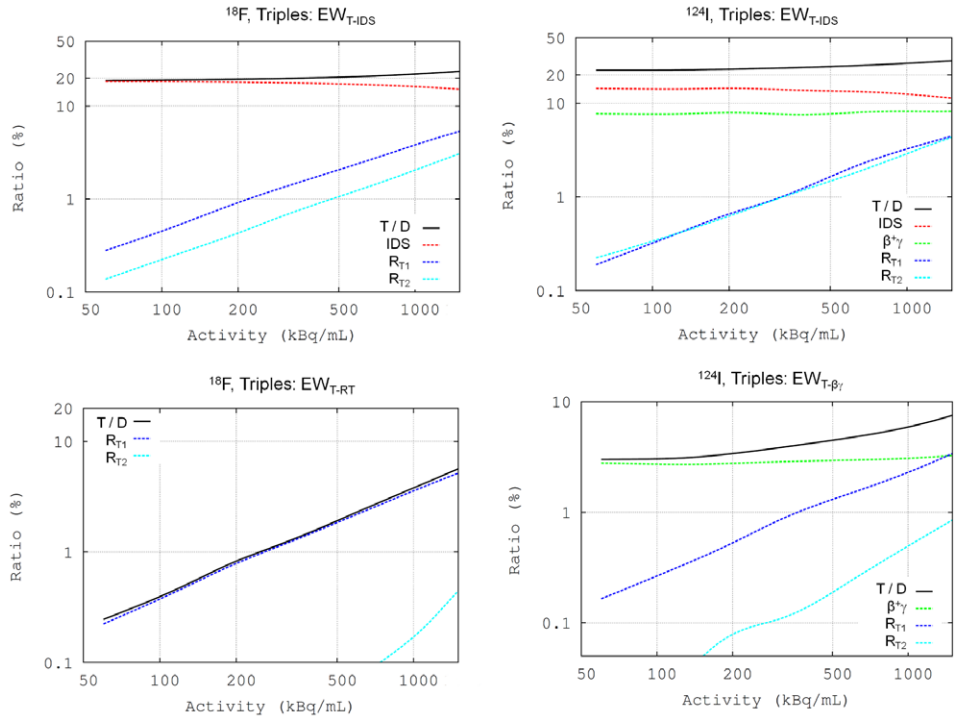

Figure 4. Simulated triples-to-doubles ratios in the Argus scanner for ^{18}F (left) and ^{124}I (right) as a function of the activity concentration within the FOV and the energy window. T/D is the total triples-to-doubles ratio in the energy window specified. IDS, $\beta^+\gamma$, R_{T1} and R_{T2} are the individual components of the triples-to-doubles ratio.

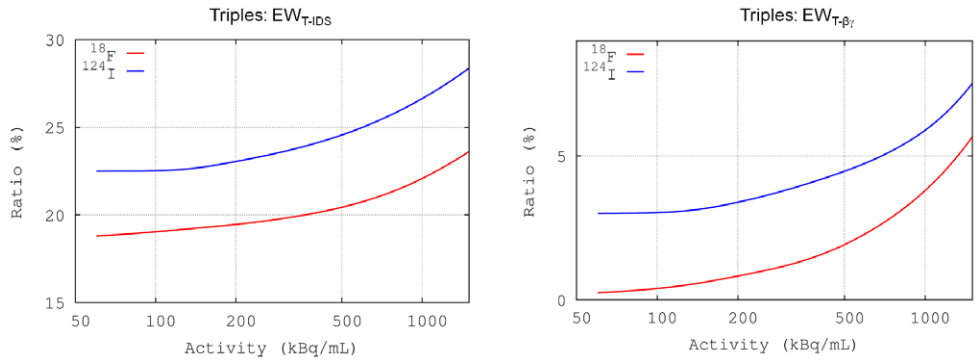

Figure 5. Simulated triples-to-doubles ratios as a function of the activity concentration for ^{18}F and ^{124}I in the EWT-IDS (left) and EWT-$\beta\gamma$ (right) energy windows.

(LOR) may be the one recorded by the scanner or the one defined by the photon which was filtered by the scanner's energy window (1–2 or 1–3 in (figure 1(d))). For R_T events and non-pure positron emitters with a prompt gamma energy close to 511 keV (i.e. ^{124}I or ^{76}Br), we may have three photons within the scanner energy window. A triple event of this type, if processed as a set

Table 6. Counting statistics of double and triple coincidences for ^{68}Ga, ^{82}Rb, ^{94m}Tc and ^{86}Y (Argus scanner).

Energy window0	Type of coincidence	^{68}Ga (3.5MBq)	^{82}Rb (3.5MBq)	^{94m}Tc (3.5MBq)	^{86}Y (3.5MBq)
EW_D	Doubles (kcps MBq^{-1})	8.4 ± 0.5	8.5 ± 0.5	6.4 ± 0.3	4.29 ± 0.23
	Trues (%)	87.4	85.6	76.2	45.6
	Scatter (%)	11.5	11.6	11.1	8.0
	Doubles $\beta^+\gamma$ (%)	0.2	1.9	11.7	45.2
	R_D (%)	0.9	0.9	0.9	1.2
$EW_{T\text{-}IDS}$	Triples Sim (kcps MBq^{-1})	1.60 ± 0.11	1.69 ± 0.11	1.60 ± 0.11	1.54 ± 0.11
	IDS (%)	96.8	90.4	63.7	35.3
	$\beta^+\gamma$ (%)	0.6	6.7	33.3	61.6
	R_{T1} (%)	1.8	1.9	1.8	1.7
	R_{T2} (%)	0.8	1.0	1.2	1.4
$EW_{T\text{-}RT}$	Triples Sim (kcps MBq^{-1})	0.026 ± 0.006	0.049 ± 0.009	0.137 ± 0.014	0.223 ± 0.020
	$\beta^+\gamma$ (%)	12.5	48.1	89.1	95.1
	R_{T1} (%)	87.1	51.3	9.8	3.7
	R_{T2} (%)	0.4	0.6	1.1	1.2
$EW_{T\text{-}\beta\gamma}$ (^{68}Ga, ^{82}Rb, ^{94m}Tc)	Triples Sim (kcps MBq^{-1})	0.005 ± 0.002	0.043 ± 0.006	0.206 ± 0.020	—
	$\beta^+\gamma$ (%)	55.8	87.0	93.8	—
	R_{T1} (%)	43.2	12.0	4.9	—
	R_{T2} (%)	1.0	1.0	1.3	—
$EW_{T\text{-}\beta\gamma}$ (^{86}Y)	Triples Sim (kcps MBq^{-1})	—	—	—	0.50 ± 0.04
	$\beta^+\gamma$ (%)	—	—	—	94.9
	R_{T1} (%)	—	—	—	3.7
	R_{T2} (%)	—	—	—	1.4

of double coincidences without special consideration, will be give added as 2 or 3 two double events coincidences (along the LORs defined by the three interaction points), thus introducing wrong information since, at most, only one of these LORs is giving positional information.

In order to evaluate the importance of triple coincidences in the aforementioned cases, we assumed in a set of simulations that the clinical scanners simply process the data looking for valid coincidence pairs within energy and timing windows. In this way, all possible valid combinations of single events pertaining to a triple coincidence with at least two photons within the timing and energy windows would be added to the doubles dataset, and assigned to the corresponding LOR defined by the corresponding interaction points.

Figure 7 shows the amount of triple coincidences which would be processed as double coincidences in the clinical scanners as a function of the activity concentration. In table 7 we present detailed information about the proportion of double coincidences which came from each type of triple coincidence for different radionuclides. Figure 7 and table 7 collectively show that for a pure positron emitter like ^{18}F the rate of triple coincidences that

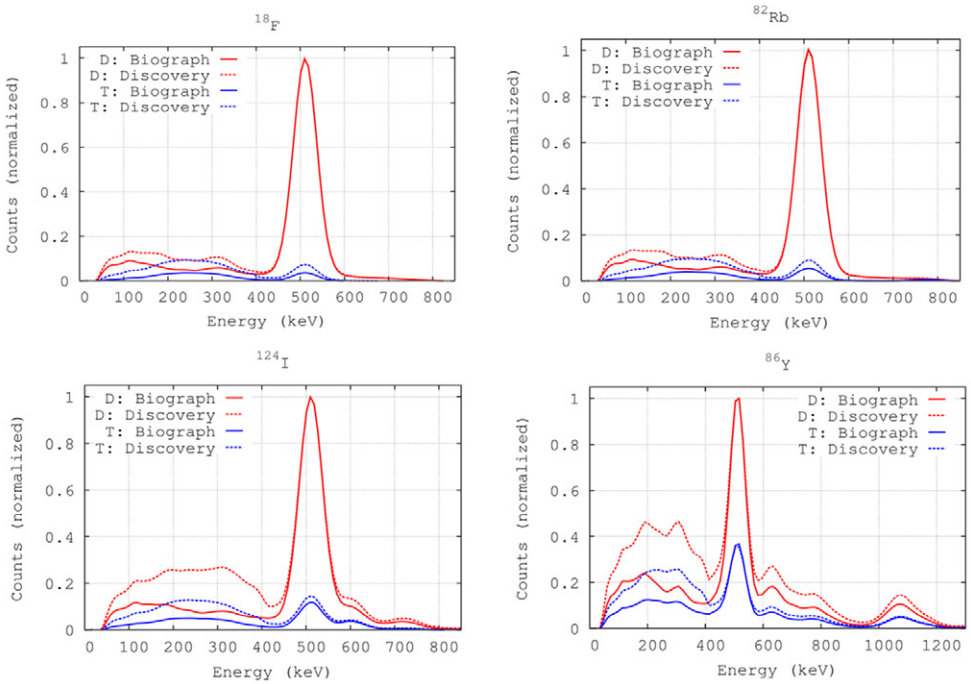

Figure 6. Simulated energy spectra for double (red) and triple (blue) coincidences in the Biograph TPTV (solid lines) and the Discovery-690 (dashed lines) scanners. The radionuclides simulated are from left to right and from top to bottom: ^{18}F, ^{82}Rb, ^{124}I and ^{86}Y. Spectra have been scaled to a value of 1 in the photopeak energy (511 keV) for double coincidences.

would be erroneously recorded as double coincidences is low at moderate activity concentrations (around 7% at 0.5 kBq ml^{-1}) increasing at high activity due to the increment of the R_T event rate. However, when non-pure positron emitters such as ^{124}I or ^{86}Y are used, the simulator shows a significant proportion of triple events processed as doubles (~25 and ~50% for ^{124}I and ^{86}Y, respectively) even at moderate activity concentrations (0.5 kBq ml^{-1}).

Table 8 summarizes counting statistics for triple coincidences in the clinical scanners. These data can be directly compared with the values obtained from the Argus preclinical scanner (tables 5 and 6). For the pure positron emitter ^{18}F, the IDS-to-double events ratio in the Biograph scanner (~14%) is lower than that found in the preclinical system (~18%) and in the Discovery scanner (~22%). This reflects the fact that IDS depends on the geometry of the scanner, and scanners with larger block detectors will have lower IDS. It is noticeable that the influence of prompt gamma emissions in the rate of triple events is much more significant in clinical systems, due to the better efficiency of their detectors at higher energies. Finally, it is also noteworthy that the amount of events in the doubles dataset for ^{86}Y is much higher in the Discovery than in the Biograph (tables 7 and 8), despite of the higher sensitivity of the Biograph scanner (table 3). This is because in the Biograph only 25 of 48 detectors per ring are in coincidence, while in the Discovery all detectors are in coincidence with each other and consequently, many events at the edge of the FOV will be discarded in the Biograph and stored in the Discovery.

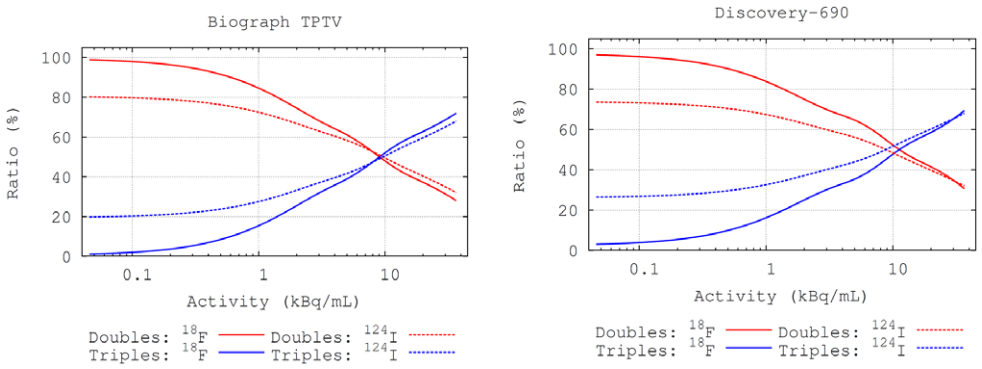

Figure 7. Percentage of actual double coincidences (doubles) and LORs coming from triple coincidences (triples) added to the doubles dataset at different activity concentrations for ^{18}F and ^{124}I. The simulation assumed that clinical scanners do not process triple coincidences in a special way and all possible valid pairs of single events were counted in the doubles dataset. In the simulations we used the NEMA Phantom (see section 2.3.3) and assumed that the scanner is using the standard energy windows for doubles (EWD, see section 1.3.1).

Table 7. Double coincidences and LORs coming from triple coincidences which are processed as doubles in the clinical scanners (^{18}F, ^{124}I and ^{86}Y).

	Biograph TPTV / Discovery-690		
	^{18}F (10 MBq)	^{124}I (10 MBq)	^{86}Y (10 MBq)
Total (kcps MBq^{-1})	2.12 ± 0.10 / 1.92 ± 0.09	0.95 ± 0.04 / 1.29 ± 0.05	2.75 ± 0.10 / 5.00 ± 0.18
Doubles (kcps MBq^{-1})	1.96 ± 0.10 / 1.74 ± 0.09	0.73 ± 0.04 / 0.91 ± 0.05	1.37 ± 0.07 / 2.32 ± 0.12
Trues (%)	54.1 / 52.5	30.2 / 19.9	14.7 / 6.9
Sc (%)	39.6 / 37.8	28.9 / 22.9	19.5 / 12.3
Doubles $\beta^+\gamma$ (%)	0.0 / 0.0	34.9 / 51.1	61.7 / 77.8
R_D (%)	6.3 / 9.7	6.0 / 6.1	4.1 / 3.0
Triples counted as doubles (kcps MBq^{-1})	0.150 ± 0.009/ 0.175 ± 0.010	0.210 ± 0.012 / 0.37 ± 0.02	1.39 ± 0.07 / 2.68 ± 0.14
IDS (%)	25.7 / 28.6	16.3 / 5.9	9.8 / 2.5
$\beta^+\gamma$ (%)	0.0 / 0.0	67.6 / 81.3	81.3 / 90.8
R_{T1} (%)	51.9 / 49.9	8.8 / 8.2	4.1 / 4.1
R_{T2} (%)	22.4 / 21.5	7.3 / 4.6	4.9 / 2.6

4. Discussion and conclusions

The new version of the MC simulation tool PeneloPET is able to accurately reproduce the behavior of several preclinical and clinical scanners when working in standard PET mode (figure 2 and tables 2 and 3). Moreover, we used real data from the Argus scanner to validate the new module of the simulator for tracking multiple coincidences and obtained deviations smaller than 10% between simulated and measured data for energy spectra (figure 3 and table 4) and most triple-to-double ratios (table 5).

After this validation, we used our code to evaluate the relative proportion of each type of triple coincidences in different scenarios for the Argus scanner and for two clinical scanners.

Table 8. Counting statistics for double and triple coincidences in the clinical scanners (^{18}F, ^{124}I and ^{86}Y).

E window	Type of coincidence	Biograph TPTV / Discovery-690		
		^{18}F (10 MBq)	^{124}I (10 MBq)	^{86}Y (10 MBq)
EW_D	Doubles (kcps MBq^{-1})	1.96 ± 0.10 / 1.74 ± 0.09	0.73 ± 0.04 / 0.91 ± 0.05	1.37 ± 0.07 / 2.32 ± 0.12
$EW_{T\text{-}IDS}$	Triples (kcps MBq^{-1})	0.271 ± 0.014 / 0.38 ± 0.02	0.187 ± 0.100 / 0.303 ± 0.016	1.05 ± 0.05 / 1.56 ± 0.08
	IDS (%)	71.0 / 79.2	21.4 / 19.7	4.0 / 3.4
	$\beta^+\gamma$ (%)	<0.1 / <0.1	63.5 / 70.7	86.0 / 90.1
	R_{T1} (%)	20.4 / 17.7	8.8 / 7.9	6.3 / 5.9
	R_{T2} (%)	8.6 / 3.1	6.3 / 1.7	3.7 / 0.6
$EW_{T\text{-}RT}$	Triples (kcps MBq^{-1})	0.012 ± 0.001 / 0.007 ± 0.001	0.017 ± 0.002 / 0.017 ± 0.002	0.074 ± 0.005 / 0.116 ± 0.007
	$\beta^+\gamma$ (%)	<0.1 / <0.1	82.3 / 84.7	89.5 / 92.9
	R_{T1} (%)	99.3 / 99.2	13.9 / 14.5	7.2 / 6.3
	R_{T2} (%)	0.7 / 0.8	3.8 / 0.8	3.3 / 0.8
$EW_{T\text{-}\beta\gamma}$ (^{124}I, ^{86}Y)	Triples (kcps MBq^{-1})	—	0.030 ± 0.002 / 0.041 ± 0.003	0.256 ± 0.014 / 0.38 ± 0.02
	$\beta^+\gamma$ (%)	—	80.1 / 86.1	89.5 / 92.4
	R_{T1} (%)	—	14.7 / 12.6	6.6 / 6.8
	R_{T2} (%)	—	5.2 / 1.3	3.9 / 0.8

In all the cases, the relative proportion of each type of triple coincidence has been shown to be closely related to the specific radionuclide being used (tables 5–8) and, for R_T events, with the activity concentration within the FOV (figures 5 and 7). For clinical scanners, we evaluated the rate of triple coincidences that would be processed as double events assuming that the coincidence processor of these scanners does not discard single photons involved in triple coincidences. We evaluated these variables for radionuclides emitting different percentages of extra gamma photons: ^{18}F (pure emitter), ^{124}I (non-pure, moderate amount of additional gamma photons per decay) and ^{86}Y (non-pure, large amount of additional gamma photons emitted per decay). Figure 7 and table 7 show that while the standard acquisition settings of PET scanners works well for pure positron emitters at low and medium activity concentrations, the rate of triple coincidences included in the double events dataset can be very important for non-pure positron emitters (contamination in the doubles dataset from triple coincidences ranged from 22 to 30% for ^{124}I and was higher than 50% for ^{86}Y). These results indicate that detecting and properly processing or discarding triple coincidences may help to improve the IQ of PET scanners when imaging radiotracers labeled with non-pure positron emitters.

Regarding possible applications of triple coincidences, this work shows that for pure positron emitters like ^{18}F it is possible to effectively detect and identify IDS and R_T events. This means that in block-detector based scanners, detection and recovery of these events (IDS and R_{T1} events define a valid line of response, as shown in figure 1) holds the potential to substantially increase the sensitivity of the scanner, if an effective method to recover these events is used. For example, sensitivity for ^{18}F in the Argus scanner can be increased on about a 24% at 700 kBq ml^{-1} by recovering IDS and R_{T1} events (figure 5). For most non-pure positron emitters studied in this work, the Argus scanner could also recover IDS and R_T events based on the same criterion, although in this case there will be around a 30% contamination due to

$\beta^+\gamma$ events in these datasets (tables 5 and 6). Interestingly, due to the differences in detector designs when using non-pure emitters in the clinical scanners (table 8) most of the events detected within the $EW_{T\text{-}IDS}$ energy window come from $\beta^+\gamma$ events. For other applications requiring the detection of $\beta^+\gamma$ events such as multiplexed PET imaging, (Andreyev and Celler 2011, Sitek *et al* 2011, Andreyev *et al* 2012, Parot *et al* 2013), our work shows that, in clinical scanners, triple-to-double ratios for these events may be of up to 4% with ^{124}I and up to 15% with ^{86}Y if we use triple coincidences within $EW_{T\text{-}\beta\gamma}$.

Acknowledgments

We thank the referees for their useful comments. This work was supported by Consejería de Educación, Juventud y Deporte de la Comunidad de Madrid (Spain) through the Madrid–MIT M+Visión Consortium. Part of the calculations were performed in the 'Clúster de Cálculo de Alta Capacidad para Técnicas Físicas' funded by UCM and by UE under the FEDER program. This is a contribution to the Moncloa Campus of International Excellence.

References

Abushab K M, Herraiz J L, Vicente E, España S, Vaquero J J, Jakoby B W and Udias J M 2011 PeneloPET simulations of the Biograph ToF clinical PET scanner *IEEE NSS MIC Conf. Record (Valencia, Spain)* pp 4420–8

Agostinelli S 2003 GEANT4—a simulation toolkit *Nucl. Instrum. Methods Phys. Res.* A **506** 250–303

Allison J *et al* 2006 Geant4 developments and applications *IEEE Trans. Nucl. Sci.* **53** 270–8

Andreyev A and Celler A 2011 Dual-isotope PET using positron–gamma emitters *Phys. Med. Biol.* **56** 4539–56

Andreyev A, Sitek A and Celler A 2012 EM reconstruction of dual isotope PET with staggered injections and prompt gamma positron emitters *IEEE NSS MIC Conf. Record* pp 4420–8

Badawi R D, Kohlmyer S G, Harrison R L, Vannoy S D and Lewellen T K 2000 The effect of camera geometry on singles flux, scatter fraction and trues and randoms sensitivity for cylindrical 3D PET—a simulation study *IEEE Trans. Nucl. Sci.* **47** 1228–32

Baró J, Sempau J, Fernández-Varea J M and Salvat F 1995 PENELOPE: an algorithm for Monte Carlo simulation of the penetration and energy loss of electrons and positrons in matter *Nucl. Instrum. Methods Phys. Res.* B **100** 31–46

Beattie B J, Finn R D, Rowland D J and Pentlow K S 2003 Quantitative imaging of bromine-76 and yttrium-86 with PET: a method for the removal of spurious activity introduced by cascade gamma rays *Med. Phys.* **30** 2410–23

Belov V V, Bonab A A, Fischman A J, Heartlein M, Calias P and Papisov M I 2011 Iodine-124 as a label for pharmacological PET imaging *Mol. Pharm.* **8** 736–47

Bettinardi V, Presotto L, Rapisarda E, Pichio M, Gianolli L and Gilardi M C 2011 Physical performance of the new hybrid PET/CT Discovery-690 *Med. Phys.* **38** 5394–411

Buvat I and Lazaro D 2006 Monte Carlo simulations in emission tomography and GATE: an overview *Nucl. Instrum. Methods Phys. Res.* A **569** 323–29

Clerk-Lamalice J, Bergeron M, Thibaudeau C, Fontaine R and Lecomte R 2012 Evaluation of easily implementable inter-crystal scatter recovery schemes in high-resolution PET imaging *IEEE NSS MIC Conf. Record (Anaheim, CA, USA)* pp 2196–9

España S, Herraiz J L, Vicente E, Vaquero J J, Desco M and Udias J M 2009 PeneloPET, a Monte Carlo PET simulation tool based on PENELOPE: features and validation *Phys. Med. Biol.* **54** 1723–42

Gillam J E, Solevi P, Oliver J F and Rafecas M 2012 Inclusion of inter crystal scatter data in PET *9th IEEE Int. Symp. on Biomedical Imaging (ISBI)* pp 62–5

Gillam J E, Solevi P, Oliver J F, Casella C, Heller M, Joram C and Rafecas M 2014 Sensitivity recovery for the AX-PET prototype using inter-crystal scattering events *Phys. Med. Biol.* **59** 4065–83

Harpen M D 2004 Positronium: review of symmetry, conserved quantities and decay for the radiological physicist *Med. Phys.* **31** 57–61

Hayden C H, Casey M E and Watson C C 2011 Prompt gamma correction for non-standard isotopes in a PET scanner *US Patent 7,894,652*

Jakoby B W, Bercier M Y, Watson C C, Bendriem B and Townsend D W 2009 Performance characteristics of a new LSO PET/CT scanner with extended axial field of view and PSF reconstruction *IEEE Trans. Nucl. Sci.* **56** 633–9

Jan S *et al* 2004 GATE: a simulation toolkit for PET and SPECT *Phys. Med. Biol.* **49** 4543–61

Jan S *et al* 2011 GATE V6: a major enhancement of the GATE simulation platform enabling modelling of CT and radiotherapy *Phys. Med. Biol.* **56** 881–901

Kacperski K and Spyrou N M 2005 Performance of three-photon PET imaging: Monte Carlo simulations *Phys. Med. Biol.* **50** 5679–95

Krane K S 1987 *Introductory Nuclear Physics* (New York: Wiley)

Lage E, Parot V, Dave S R, Udias J M, Moore S C, Sitek A, Park M-A, Vaquero J J and Herraiz J L 2014 Recovery and normalization of triple coincidences in PET *Med. Phys.* submitted

Levin C S 2008 New imaging technologies to enhance the molecular sensitivity of positron emission tomography *Proc. IEEE* **96** 439–67

Lewellen T K 2008 Recent developments in PET detector technology *Phys. Med. Biol.* **53** R287–317

Lin H, Chuang K, Chen S, Chiang C, Lin C and Jan M 2012 Recycling of triple coincidences for non-pure positron emitters in MiroPET imaging *Eur. J. Nucl. Med. Mol. Imaging* **39** S155–303

Lubberink M and Herzog H 2011 Quantitative imaging of ^{124}I and ^{86}Y with PET *Eur. J. Nucl. Med. Mol. Imaging* **38** 510–518

Lubberink M, Schneider H, Bergström M and Lundqvist H 2002 Quantitative imaging and correction for cascade gamma radiation of 76Br with 2D and 3D PET *Phys. Med. Biol.* **47** 3519–34

NNDC 2011 National Nuclear Data Center, Brookhaven National Laboratory (www.nndc.bnl.gov/)

NEMA NU-2 2007 *Performance Measurements of Positron Emission Tomographs* (Rosslyn, VA: National Electrical Manufacturers Association)

NEMA NU-4 2008 *Performance Measurements for Small Animal Positron Emission Tomographs* (Rosslyn, VA: National Electrical Manufacturers Association)

Panettieri V, Wennberg B, Gagliardi G, Duch M A, Ginjaume M and Lax I 2007 SBRT of lung tumours: Monte Carlo simulation with PENELOPE of dose distributions including respiratory motion and comparison with different treatment planning systems *Phys. Med. Biol.* **52** 4265–81

Parot V, Herraiz J L, Dave S R, Udias J M, Moore S C, Park M-A, Vaquero J J and Lage E 2013 A new approach for multiplexed PET imaging *IEEE NSS-MIC 2013* (Seoui, South Korea)

Rafecas M, Böning G, Pichler B J, Lorenz E, Schwaiger M and Ziegler S I 2003 Inter-crystal scatter in a dual layer, high resolution LSO-APD positron emission tomograph *Phys. Med. Biol.* **48** 821–48

Robinson S, Julyan P J, Hastings D L and Zweit J 2004 Performance of a block detector PET scanner in imaging non-pure positron emitters-modelling and experimental validation with ^{124}I *Phys. Med. Biol.* **49** 5505–28

Salvat F, Fernández-Varea J M and Sempau J 2008 PENELOPE-2008—a code system for Monte Carlo simulation of electron and photon transport NEA-OCDE *Workshop Proc. (30 June-3 July 2008, Barcelona, Spain)*

Sempau J and Andreo P 2006 Configuration of the electron transport algorithm of PENELOPE to simulate ion chambers *Phys. Med. Biol.* **51** 3533–48

Sitek A, Andreyev A and Celler A 2011 Reconstruction of dual isotope PET using expectation maximization (EM) algorithm *IEEE NSS MIC Conf. Record* (*Valencia, Spain*) pp 4323–6

Surti S, Scheuermann R and Karp J S 2009 Correction technique for cascade gammas in I-124 imaging on a fully-3D, time-of-flight PET scanner *IEEE Trans. Nucl. Sci.* **56** 653–60

Wagadarikar A A, Ivan A, Dolinsky S and McDaniel D L 2012 Sensitivity improvement of time-of-flight (TOF)-PET detector through recovery of compton scattered annihilation photons *IEEE NSS MIC Conf. Record* (*Anaheim, CA, USA*) pp 3178–83

Wang Y, Seidel J, Tsui B M W, Vaquero J J and Pomper M G 2006 Performance evaluation of the GE healthcare eXplore VISTA dual-ring small-animal PET scanner *J. Nucl. Med.* **47** 1891–900

Zanzonico P 2004 Positron emission tomography: a review of basic principles, scanner design and performance, and current systems *Semin. Nucl. Med.* **34** 87–111